Early Detection of Brain Tumors Using SOLOv3 Algorithm for Enhanced Diagnostic Accuracy

[1*]Sindhu S, [2]Vijayalakshmi N,
[1,2]Department of Computer Applications, SRM Institute of Science & Technology, Ramapuram, Chennai, India
E-mail: sindhus1@srmist.edu.in
[*]Corresponding author

Keywords: brain tumor, SOLOv3, machine learning, classification

Received: December 18, 2024

The brain tumor is various types occur in the human brain sometime it affects the human quality of life. The deep learning algorithms gives the better detection of the tumor cell with highly positive result in the earlier stage. In the previous work, the customized Segmenting Objects by Locations Vector 3(SOLOv3) algorithm has been approached, this approach gives the better result compared with the previous algorithms. In the medical field the radiographic images are plays the vital role for identifying the disease from the human body at the same time helps to give the proper treatment on time for avoiding the death ratio. There are many automatic image reorganization techniques were developed in deep learning algorithms. Since the proposed idea is to classify the images based on the plasma level and also detect the levels of infection specified as stage1 to stage 5. To use the Magnetic Resonance Images (MRI) for identifying the tissues which present the human organ with the neoplasm type and size. This kind of information's are helpful to treat the patient on time and also reduce the death rate due this late treatment or detection of the which level the person may affected. The aim of the proposed article is to develop the customized SOLOv3 algorithm with DESNET201 for improved image segmentation and classification. The real time images were taken from the prescribed reputed Neurological diagnosis center in Chennai. Totally 18759 images were collected under all four categories of tumor and non tumor. Which included 13257 images are tumor images under the category of glioma, meningioma and pituitary and remains comes under non tumor category. The implemented model is to customize the final layer of the neural network form with four different classes will give the better result as 91% in the training set and scored 89% as in the phase of test. This improved model that could combine the SOLOv3 and Desnet201 with customized layer classes for extracting the features used to classify the tumor cells with their different types. The tumor may have more than 150 types of tissues, but gradually these four kinds of classes are very dangerous about to increase the death and spreadable to other body organ. These techniques also able to detect the improved automation for the tumor in Indian children and adults.

Povzetek: Prispevek združuje algoritma SOLOv3 in DenseNet201 za zgodnje odkrivanje možganskih tumorjev iz MRI posnetkov ter poroča o izboljšani segmentaciji in klasifikaciji v pet razredov tumorjev.

1 Introduction

In recent years, sedentary behavior has emerged as the brain is the vital organ that governs the functioning of the entire human body. The brain provides instructions to other organs to do their respective functions without any interruption. The nervous system typically regulates the functions of the human body by transmitting signals to various components of the human organism. When the brain is in a healthy state, all human activities will be normal. Conversely, if the brain is in an unhealthy condition, all activities will be abnormal. The brain can become compromised by a range of factors, including tumors, genetic abnormalities, injuries, or familial problems. This article presents a novel approach for identifying cancerous cells in the brain. If the tumor cell is found early, it may be possible to remove it, even though there may not be a treatment for many causes. The explanation provided was thorough and focused on both the desired result and the practical application, with particular emphasis on the loss function. A brain tumor is an abnormal proliferation of tissues that originate and spread inside the human body, affecting other organs [1]. Tumors of different

sorts arise in the human brain and are categorized according to the dimensions and morphology of the cells in the affected region [2]. The provided (Figure 1) displays normal brain imaging on the left side and brain tumor pictures on the right side. Figure 1 displays two distinct brain types, one with an unhealthy tumor image on the left and a healthy brain image on the right. These images were obtained from MRI scans.

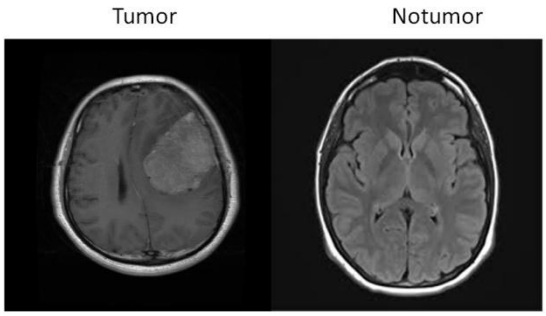

Figure 1: MRI scan comparison of a brain with a tumor (left) and a healthy brain (right).

According to the World Health Organization, there are around 150 different varieties of brain tumors. Not all types of tumors are dangerous to human life, since some are classified as low-grade. Certain cancers are classified as high-grade and pose a significant threat to human life. There are fewer than four types. It exhibits rapid proliferation and metastasis to both cerebral tissues and other bodily organs. It impairs cognitive function and leads to a decline in mental capacity. Living the regular life of a human might have detrimental effects. The primary procedure of the proposed project will be carried out in three distinct phases.

The initial and most important phase is image processing. At this stage, the image has undergone processing at two distinct levels: pre-processing involving the application of fundamental noise reduction techniques, background separation, and other related procedures. The subsequent stage is post-processing, which will focus on the consolidation of the tissues or cyst, which may be diminutive and irregular in shape.

Figure 2 depicts the alterations of both normal brain cells and malignant cells. The typical cell is correctly arranged and tightly packed without any gaps, exhibiting a desirable form and size. The tumor cells have atypical morphology and dimensions; they may aggregate in clusters or exist individually.

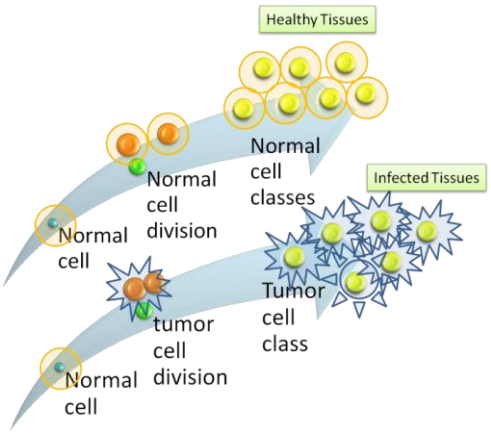

Figure 2: Sample images normal cell versus tumor cell in the brain

Next, the features will be extracted from the images in order to apply the PCS-GIST method and RLEM methods for feature identification. The characteristics are as follows:

- Pixel value
- Contrast level
- Color value
- Texture rate
- Relational pixel value

Tumors originating in the brain and other nervous systems are the 10th leading cause of death and the third most common cancer in both young people and adults [2]. Imaging is the primary approach for accurately diagnosing disorders within the internal organs and achieving accurate results. Multiple imaging systems are accessible, including ultrasound, reverberation imaging, and tomography techniques [3].

Magnetic resonance imaging (MRI) is the most effective approach for detecting diseases, assessing the extent of damage, and evaluating illness severity. This technique automatically eliminates noise and provides superior tissue contrast. Artificial intelligence techniques are employed to examine photos and analyze their characteristics in order to diagnose certain qualities of each image, including pixel value, color value, texture, and correlation points [3]. The deep learning algorithm model [4] and [5] were created to extract image features. They were applied with various mathematical computations and references to identify the picture features. The model also discovered the correlated points of each feature with good performance. The neural network was constructed with multiple layers, each utilizing their respective classes and numerical approaches. At that juncture, the image focuses on a conduit that selectively

removes insignificant attributes and converts the remaining ones into a display that is reduced in size compared to its previous form.

2 Literature review

This section explores different deep learning segmentation techniques used for implementing a 3-dimensional (3-D) magnetic resonance imaging (MRI) image. Recently, numerous authors who have contributed to image segmentation research in IEEE and Scopus-indexed publications have undergone evaluation. [1] The research involved identifying tumor cells in brain MRI images by utilizing the active contour approach to locate specific regions of interest. [2] The author employed the convolutional neural network (CNN)-based image encoder technique to eliminate undesirable characteristics. This method was then utilized to partition the image and detect the tumor area in the brain images. The user's text is "[3]". The objective of the research is to execute the use of five pre-trained models: ResNet50, Inception V3, MobileNet101, and Xceptions. This architecture can be better understood by its effective implementation. The photos are classified based on glioma and pituitary tumor cells using the F1 score, loss functions, and loss error, with the best accuracy. [4] this paper used the GoogleNet and RestNet50 algorithm for detection of infected region without proper dataset. [5] This work utilized median filtering approaches for image processing and focused on using the texture method for feature extraction. Additionally, a CNN model was employed for cancer detection. [6] The author has utilized the classification technique to categorize tumor photos into tagged images belonging to either the tumor or non-tumor class. [7] The tumor cell classification concept employs the CNN algorithm. The author utilized the Kaggle repository dataset for their research. [8] The photographs were enhanced by their enlarged dimensions and form. [9] This study proposes a CNN-based classification approach for analyzing MRI images to determine the presence or absence of a tumor. The obtained outcome is contrasted with the suggested approach. [10] The tumor photos were inputted into the model in order to generate synthetic data for enhanced model training and testing [11]. The author used the BrsTS22D dataset into a sparse-stacked auto-encoder model to efficiently identify the infected region cell in a minimal amount of time. [12] Tumor cells are interconnected with different organs in the body. The majority of the research has focused on the deep learning network, specifically examining its many layers [13, 14]. The objective of this study is to enhance image segmentation and classification by utilizing the most effective deep learning network algorithm, specifically the customized SOLOv3 algorithm with DESNET201. This approach is expected to yield superior results compared to other algorithms [15]. In 2020, the author delivered a presentation at an international conference where they highlighted their study on classifying tumor cells in the brain using MRI scans. They explained and implemented several deep learning models, including Inspection108, RestNet50, VGG32, Xception, and MobileNet101 [16]. Automate the process of segmenting brain tumor images during the scanning conducted by the investigators. The radiologist use magnetic resonance imaging techniques to identify the stage of tumors and assess the levels of infection. In 2023, there were 150 distinct tumor types accessible. The objective is to focus on the multi-class classification of each specific type of tumor cell. In order to identify the 109 distinct categories for the classification of tumor cells, as utilized in the proposed study. However, when it comes to tasks that involve dividing medical images into segments, the DenseNet-201 (Dense Convolutional Network-201) architecture is highly effective. There are numerous parameters, which might result in a significant amount of computational work during both inference and training. Due to its complex structure and several variables, there is a higher risk of overfitting when sparse or small datasets of medical images are used. Decreased performance on newly taken photographs is caused by overfitting, a phenomenon that occurs when the model becomes too focused on memorizing the training data rather than being able to apply its knowledge to new, unseen data.

3 Proposed work

The feature extraction model utilizes auto-encoders to identify any corrupted samples within the undamaged data. This study presents a novel approach to edge identification using evolutionary algorithms, which improves the accuracy and effectiveness of the model. The raw image of the patient's brain was obtained and could be subjected to processing in order to prevent both under fitting and over fitting of the DesNet201 model. The DesNet201 algorithm analyzes the image (Figure 3) to accurately determine the precise location of tumor tissues in the brain. It also identifies the size and shape of the tumor, as well as the extent to which it has been affected by other organs. The segmented image was utilized to categorize the different sorts of tumors into numerous classifications such as glioma, pituitary, malignant, and others.

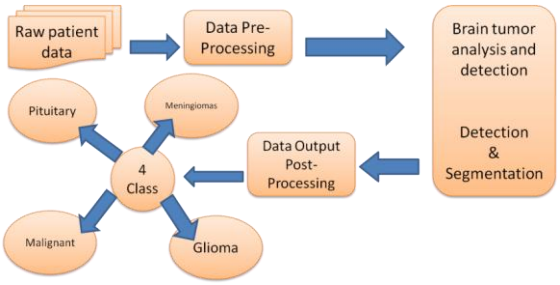

Figure 3: represents the work flow of the proposed systems

The genetic algorithm is employed to delineate the boundaries of the processed image in order to identify the subsequent region of tissues encountered in the same situation. The genetic algorithm efficiently identifies the edges. Typically, it proceeds via three distinct stages. During the initial phase, the skull is meticulously removed to separate the brain tissues and non-brain tissues from the MRI pictures. This is done in order to facilitate subsequent analysis.

The image contrast has been adjusted and improved from the unprocessed dataset [21], a publication published in 2022. The genetic method utilizes a Visually Geometry Group (VGG)-based Symmetric Convolutional Neural Network (SCNet) in conjunction with Densely Connected Convolutional Networks (DesNet) to accurately classify brain tumor images. The classifier operates using a stacked layer approach, specifically with 201 image classifications. The planned work architecture is clearly elucidated in Figure 4. The unprocessed data can be found in a recent online repository such as Kaggle and can be downloaded in png file using the HSV color model. The photos were stored in a specific area, which could be utilized for the process of image classification.

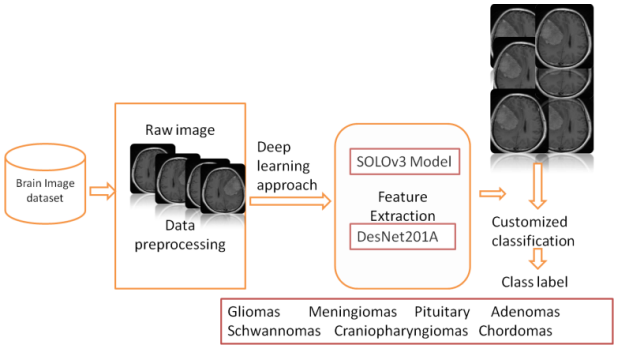

Figure 4: Architecture of the proposed work

The photos were captured at a reputable diagnostic clinic situated in Chennai. The authentic patient raw data was collected from the MedPlus neurological diagnosis facility. Approximately 29,458 images have been extracted from the raw image collection after undergoing processing to eliminate undesirable brain images and non-cleared images. Figure 5 shows the combination of tumor and non-tumor MRI image dataset.

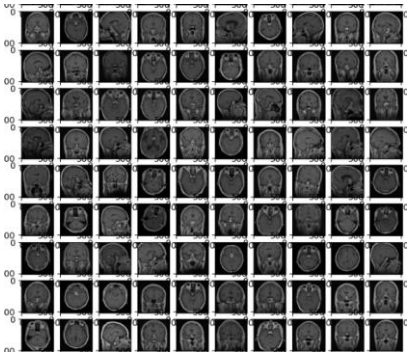

Figure 5: Combination of Tumor and non-tumor MRI image dataset

The 18759 brain-scanned images are classified into five distinct categories and are used as input. Table 1 separates the photos from the raw images in order to comprehend the distinct groups.

Table 1: Dataset classes

Classes	**Classes**	**No.of Images**
Tumor	Gliomas	8659
	Meningiomas	7854
	Pituitary Adenomas	3587
	Schwannomas:	4256
	Craniopharyngiomas	2453
	Chordomas	3765
	Schwannomas	1896
Non-tumor		**3257**

The real-time photos were captured at a renowned neurological diagnosing center in Chennai. A total of 18,759 pictures were collected across all four kinds of cancers, referred to as tumors and non-tumors. The dataset consists of 13257 photos, which are categorized as glioma, meningioma, and pituitary tumors, while the remaining images belong to the non-tumor category.

4 Methodology

The proposed work presents a comprehensive user-interactive framework for conducting various analyses on brain MRI images to aid medical professionals. Most of the framework has the capability to identify biological data pertaining to the patient. Certain tailored classes inside the deep neural network have a greater likelihood of accurately detecting the tumor based on a higher probability score. The SOLOv3 deep learning algorithm was employed for edge detection, while DesNet201 was utilized for tumor cell classification into five distinct categories.

SOLOv3 Algorithm:

The SOLOv3 algorithm is the most superior deep learning approach for detecting instances. Instance segmentation is the process of detecting and outlining separate items in an image, giving a distinct name to each object, and differentiating between objects that may overlap or block each other. Analyzing and reconstructing the image view is used to identify the edges of tumor tissue in brain electromagnetic imaging and portable head image work [21]. The article was published in the 2018 edition of the Springer journal "Brain Informatics". The SOLOv3 algorithm performs segmentation using five distinct steps according to the specified metrics. The initial and most important step is to obtain the image from the scanned video in the MP3 format. The program utilizes each frame to detect the impacted locations. The feature extraction method is performed using the convolutional neural network approach with modified network frames. The feature engineering method involves preprocessing the input.

Stage 1: Image pre-processing

During this stage, the raw image undergoes various processing steps to train the model. These steps include denoising, blurring the background, normalizing the image, and adjusting the pixel value range to be between 0 and 1. This type of preprocessing enhances the training of the model and results in a higher prediction accuracy as in figure 6.

$$\text{normalized\_pixel\_value} = \frac{\text{pixel\_value} - \text{mean}}{\text{standard\_deviation}} \quad \text{(Equation 1)}$$

Here, the image's mean pixel value is its mean. The standard deviation of the image's pixel values is called standard_deviation.

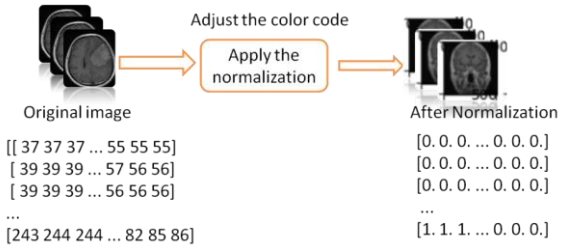

Figure 6: Input pre-processing, converting original image to normalized image

In order to standardize the pixel values within a specific range (such as [0, 1] or [-1, 1]), it is necessary to subtract the mean pixel value of the image and then divide the resulting value by the standard deviation during the normalization process. Next, it is necessary to calibrate the histogram level of each image (according to Equation 2) in order to enhance the image quality. To disperse the pixel intensities over the histogram, utilize a transformation function. Typically, this is accomplished by utilizing techniques such as contrast stretching or histogram matching. The histogram of the input image is denoted as h(i), where i represents the pixel intensity values. In the case of 8-bit images, these values range from 0 to 255. The cumulative distribution function (CDF) or CDF(i) is calculated.

$$\text{cdf}_{(i)} = \sum_{y=0}^{x} his_j \quad (2)$$

Next, T(i), the transformation function for histogram adjustment, is calculated (Equation 3).

$$T_i = \frac{\text{cdf}_i\text{-cdf}_{min}}{M \times N\text{-cdf}_{min} \times (L-1)} \quad (3)$$

The number of columns in the image is denoted by N, whereas M represents the row count of the image. The value of L, which is 256 for 8-bit images, represents the total number of intensity levels. The value of Cdf_{min} is the smallest non-zero value of the cumulative distribution function (CDF) that is used to avoid division by zero. This is seen in Figure 7.

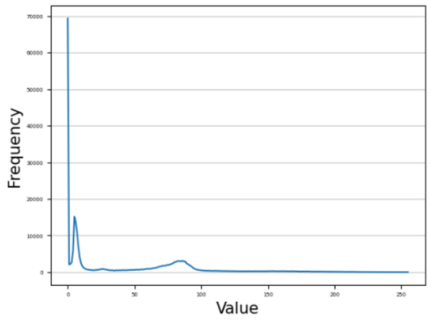

Figure 7: Histogram representation of the image to adjust the color contrast for qualifying the image predictions

Stage 2: Color scale modification & filtrations

The preprocessed image, which may be in RGB or HSV color space, is transformed into grayscale format to mitigate color contrast problems during feature detection in image segmentations. The gray-scale color contrast is deemed to possess an appropriate value. The color contrast is transformed into a grayscale image and then turned into binary format data. To remove noise from the background of the image caused by overlapping foreground elements. It eliminates the undesired borders from the image sections.

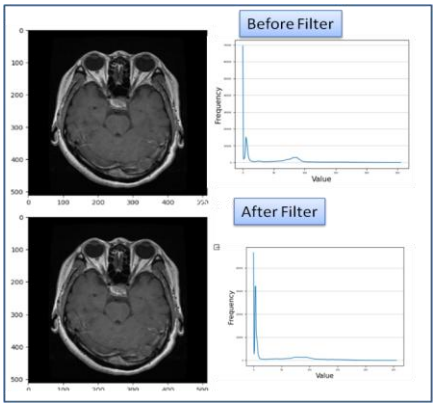

Figure 8: The image smoothing with 3.4 aspect ratio

Gaussian filtering:

Gaussian blurring is a widely used technique in image processing that reduces noise and fine details in a picture by applying a smoothing effect. The process involves applying a two-dimensional Gaussian distribution, also called a Gaussian kernel, to the image by convolution. Equation 4. The process of achieving Gaussian blurring involves applying the Gaussian kernel to every pixel in the image as in figure 8. The initial parameter to specify when applying a Gaussian filter on an image is the dimension of the kernel or matrix that will be used to degrade the image. Generally, we designate the dimensions as odd numbers, which enables us to calculate the final outcomes by utilizing the pixel in the center. Furthermore, because to their symmetry, the kernels possess an equivalent number of rows and columns. Analyze the frequency spectra (as shown in Figure 9) of the image both prior to and following the application of the filter. Gaussian filters are designed to maintain the low-frequency visual information while reducing the high-frequency noise. Employ the Fast Fourier Transform (FFT) technique to ascertain the frequency spectrum of the original image.

$$G(x,y) = \frac{1}{2\pi\sigma^2} e^{\frac{-x^2+y^2}{2\sigma^2}} \quad (4)$$

Here, x → X coordinate value, y → Y coordinates value,

σ → Standard Deviation

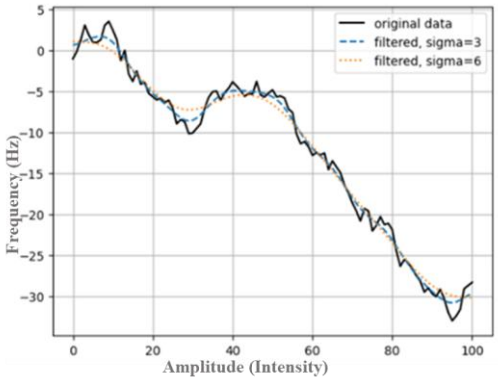

Figure 9: Gaussian filter sigma assigned by 3 and 6.

This process involves converting the spatial domain representation of the image into the frequency domain, which allows us to observe the distribution of frequencies present in the image. Apply a Gaussian kernel to perform convolution on the source image. The degree of blurring that the image undergoes is determined by the standard deviation parameter and the kernel size. Gaussian filters smooth the image by attenuating high-frequency components in the frequency domain, achieved by averaging pixel values in the spatial domain.

Stage 3: Extracting the infected region as feature

At this stage, the image has undergone processing, and each dataset has been divided into two distinct sets of data for the segmentation process. 80% of the image dataset was allocated for training the model, while the remaining photos were used to test the model's predictive accuracy. The processing frames per second (Fps) at this level are computed to complete the training phase of the model.

$$FP_s = \frac{1}{Pr\,oces\,sin\,g\_time\_per\_frame} \text{ (Equation 5)}$$

The amount of time (in seconds) that the algorithm needs to process one frame is known as the processing time per frame(Equation 5).

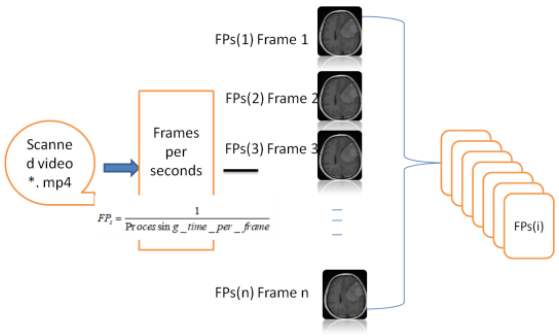

Figure 10: Image frames segment from MRI scanned video

To determine the processing time per frame, you can utilize a stopwatch or performance profiling tools, such as Figure 10, to monitor the duration it takes for the algorithm to process a batch of frames. This duration can then be divided by the total number of frames in the batch. Alternatively, you can directly compute the processing time of each individual frame. Using the initial frame calculation, the image has been extracted from the input data obtained by video scanning. The frames per second (FPS) ranges from 0 to 1, while the FPS value for a specific frame (FPS(i)) is between €1 and €0, inclusive.

Stage 4: Hyper tuning the parameter using SOLOV3

To entails determining which hyper parameter combination will yield the best results on a validation dataset. Choose a hyper parameter search method before moving on. Typical tactics include of evolutionary algorithms, random search, grid search, and Bayesian optimization. In terms of efficacy and efficiency [22], every tactic has advantages and downsides. Hyper-parameter tuning is essential for estimating the model parameters, whereas parameter tuning is crucial for producing predictions. The effectiveness of the training is determined by the selection of hyperparameters. The learning rate in gradient descent governs the efficacy and accuracy of the optimization process in parameter prediction.

Stage 5: Customized Classification with eight classes using DesNet201A

The Mask Intersection Over Union (MaskIOU) measures the degree of overlap between the segmentation mask output and the ground truth mask. The foreground image scene overlaps the background, causing confusion between the data and the image augmentations. The similarity has been identified and compared to the threshold for the more accurate forecasts as in table 2. The Mask_IoU mask interaction has been computed based on the intersection area between the predicted mask (Mpred) and the ground truth mask (Mgt), as indicated by equation 2.

Table 2: Mask interaction value predicted using the various algorithms

Classes	SOLOv2	Faster RCNN	Desnet 360	Proposed work
Gliomas	61%	62%	48%	82.4%
Meningiomas	71%	68.2%	61%	88.9%
Pituitary Adenomas	68%	58%	71%	78.2%
Schwannomas:	68.2%	61%	61%	62%
Craniopharyngiomas	61%	88.9%	71%	78.2%
Chordomas	71%	78.2%	61%	88.9%
Schwannomas	72%	68.2%	61%	79%
Non-tumors	68.2%	61%	83%	88%

5 Experimental analysis

The feature engineering process is main work for the detection of anomaly from given scan footage using MRI. The evaluation can be done with various assessment metric method and techniques.
The measurements are:

- Mean Average Precision (mAP)
- Mask Intersection over Union (Mask IoU)
- Mean IoU (mIoU)
- Pixel Accuracy
- FPS (Frames Per Second)
- Instance-Level Metrics

The initial metric for feature engineering is mean Average Precision (mAP), which quantifies the effectiveness of object identification and image segmentation in real-time. This study employed a categorization system consisting of five distinct types, including malignant, pituitary, and non-tumor, to categorize the layers. The mean average precision

value is computed by using the mean value of each class in Equation 6 for classification purposes.

$$\text{MaP}=MaP = \frac{\sum_{class=1}^{n} AP}{n} \quad (6)$$

MaP – Mean average Precision is the value of comparing the originality of a classification with various classes. n-represents the number of classes assigned for each layer for classifications. AP- represents the average precision value for class c. c-represents the classes such as malignant, pituitary, non-tumor

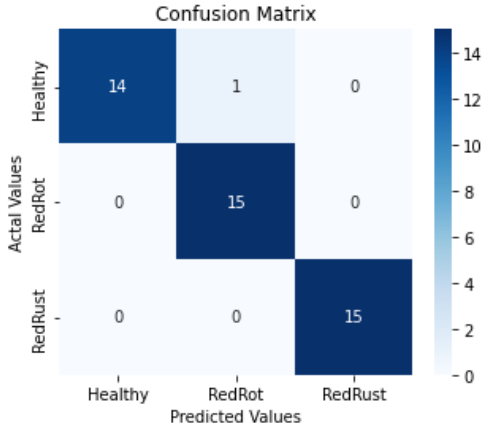

Figure 11: compares the healthy and unhealthy predicted value with confusion matrix

Each classes have its own precision value, based on this value the mean value calculated and based on that value the accuracy has been measured(Figure 11). The next level to find the accuracy of an each pixel from the Total number of pixel into correct predicted images pixel value.

$$P = \frac{N\_classified\_Correct}{N_{Total\_image}} \quad (7)$$

In equation 7: N classification correct is the number of correctly classified pixels. N_{total} is the total number of pixels in the image. A simple statistic called Pixel Accuracy (P) (as shown in Table 3) is frequently used to assess the accuracy of segmentation tasks at the pixel level, including semantic or instance segmentation. In comparison to the ground truth masks, it calculates the proportion of correctly identified pixels in the segmentation masks.

Table 3: Accuracy of a pixel with accuracy pixel value

Classes	**SOLO v2**	**Faster RCNN**	**Desnet 360**	**Proposed work**
Gliomas	0.88	0.91	0.91	0.92
Meningiomas	0.62	0.42	0.25	0.68
Pituitary Adenomas	0.52	0.58	0.69	0.47
Schwannomas:	0.42	0.24	0.36	0.37
Craniopharyngiomas	0.27	0.25	0.38	0.68
Chordomas	0.14	0.57	0.14	0.88
Schwannomas	0.74	0.74	0.77	0.77
Non-tumors	0.78	0.75	0.77	0.86

Pixel Accuracy, which is the percentage of correctly categorized pixels in the segmentation masks, offers a straightforward indicator of overall segmentation performance. Nevertheless, it does not distinguish between different types of errors (e.g., false positives vs. false negatives) or take into consideration class imbalance. Because of this, it is frequently combined with other measures to provide a more thorough assessment.

6 Conclusion

The adoption of the SOLOv3 algorithm and DenseNet201A underscores the transformative potential of deep learning in the segmentation and classification of brain tumors. By leveraging these advanced techniques, significant strides can be made in neuro-oncology, enabling more precise diagnostic capabilities and customized treatment plans. Such advancements are particularly critical for addressing the complexity and diversity of brain tumors, which often pose challenges in timely diagnosis and intervention. The proposed model not only enhances image segmentation accuracy but also enables the effective categorization of tumor types such as gliomas, meningiomas, and pituitary adenomas, among others. By accurately identifying these tumor classes and their stages, the model supports early detection and aids in determining the optimal course of treatment.

References

[1] Khan, A.B.F., Kamalakannan, K. & Ahmed, N.S.S. Integrating Machine Learning and Stochastic Pattern Analysis for the Forecasting of Time-Series Data. SN COMPUT. SCI. 4, 484 (2023). https://doi.org/10.1007/s42979-023-01981-0.

[2] Zhang, Z., Yang, G., Zhang, Y., Yue, H., Liu, A., Ou, Y., Gong, J., & Sun, X. (2024). TMFormer: Token Merging Transformer for Brain Tumor Segmentation with Missing Modalities. Proceedings of the AAAI Conference on Artificial Intelligence, 38(7), 7414-7422. https://doi.org/10.1609/aaai.v38i7.28572.

[3] Huang, Y., Jiang, L., Han, T., Xu, S., Liu, Y., & Fu, J. (2022). High-accuracy insulator defect detection for overhead transmission lines based on improved

YOLOv5. Applied Sciences, 12(24), 12682. https://doi.org/10.3390/app122412682.

[4] Vijayalakshmi, N., Sindhu, S., & Dhilipan, J. (2021). Internet of Thing-Based Monitoring Systems and Their Applications. In Smart Computing and Self-Adaptive Systems (pp. 133-152). CRC Press.

[5] Sindhu, S., & Vijayalakshmi, N. (2024). Tools to Create Synthetic Data for Brain Images. In Applications of Synthetic High Dimensional Data (pp. 179-208). IGI Global.

[6] Reshi, A. A., & Parah, S. A. (2018, December). Performance evaluation and future scope of image secret sharing schemes. In 2018 Fifth International Conference on Parallel, Distributed and Grid Computing (PDGC) (pp. 640-645). IEEE. https://doi.org/10.1109/PDGC.2018.8745872.

[7] Fadel, M. M., Said, W., Hagras, E. A., & Arnous, R. (2023). A Fast and Low Distortion Image Steganography Framework Based on Nature-Inspired Optimizers. IEEE Access. https://doi.org/101109/ACCESS.2023.3326709.

[8] Sivasankari, R., Sindhu, S., Dhilipan, J., & Vijayalakshmi, N. (2023). Impact of Machine Learning Algorithms in Decision-Making with Serious Games in the Education and Healthcare Sectors. In Handbook of Research on Decision-Making Capabilities Improvement with Serious Games (pp. 294-310). IGI Global.

[9] Prasad, V. K., Bhattacharya, P., Maru, D., Tanwar, S., Verma, A., Singh, A., ... & Raboaca, M. S. (2022). Federated learning for the internet-of-medical-things: A survey. Mathematics, 11(1), 151. https://doi.org/10.3390/math11010151.

[10] Çınar, N., Kaya, B., & Kaya, M. (2022, March). Comparison of deep learning models for brain tumor classification using MRI images. In 2022 International conference on decision aid sciences and applications (DASA) (pp. 1382-1385). IEEE. https://doi.org/101109/DASA54658.2022.9765250.

[11] Sujatha, K., & Rao, B. S. (2023, February). Densenet201: a customized DNN model for multi-class classification and detection of tumors based on brain MRI Images. In 2023 Fifth International conference on electrical, computer and communication technologies (ICECCT) (pp. 1-7). IEEE. https://doi.org/10.1109/ICECCT56650.2023.10179642

[12] Kalejahi, B. K., Meshgini, S., & Danishvar, S. (2023). Segmentation of Brain Tumor Using a 3D Generative Adversarial Network. Diagnostics, 13(21), 3344. https://doi.org/10.3390/diagnostics13213344.

[13] Isaac, Y. Z. E., Moorthy, K., Machap, L., Mohamad, M. S., & Sallim, J. (2020, August). Gene Regulatory Network Construction of Ovarian Cancer Based on Passing Attributes between Network for Data Assimilation. In 2020 8th International Conference on Information Technology and Multimedia (ICIMU) (pp. 251-255). IEEE. https://doi.org/10.1109/ICIMU49871.2020.9243432.

[14] Mathur, M., Jindal, V., & Wadhwa, G. (2020, November). Detecting malignancy of ovarian tumour using convolutional neural network: A review. In 2020 Sixth International Conference on Parallel, Distributed and Grid Computing (PDGC) (pp. 351-356). IEEE. https://doi.org/10.1109/PDGC50313.2020.9315791.

[15] Chatterjee, S., Nizamani, F. A., Nürnberger, A., & Speck, O. (2022). Classification of brain tumours in MR images using deep spatiospatial models. Scientific Reports, 12(1), 1505.

[16] Song, H. J., Yang, E. S., Kim, J. D., Park, C. Y., Kim, Y. S., & Kyung, M. S. (2018, April). Improving performance for classifying ovarian cancer with menopause information. In 2018 IEEE International Conference on Applied System Invention (ICASI) (pp. 1222-1223). IEEE. https://doi.org/10.1109/ICASI.2018.8394509.

[17] Sung, C. Y., Huang, C. C., Chen, Y. S., & Lee, G. B. (2021, January). Extraction and quantification of microrna biomarkers for diagnosis of ovarian cancer on an integrated microfluidic platform. In 2021 IEEE 34th International Conference on Micro Electro Mechanical Systems (MEMS) (pp. 366-369). IEEE. https://doi.org/10.1109/MEMS51782.2021.9375425.

[18] F. Bray, J. Ferlay, I. Soerjomataram, R. L. Siegel, L. A. Torre, A. Jemal, "Global cancer statistics 2018: GLOBOCAN estimates of incidence and mortality worldwide for 36 cancers in 185 countries", CA: Cancer J. Clin., vol. 68, pp. 394-424, 2018.

[19] G. C. Jayson, E. C. Kohn, H. C. Kitchener, J. A. Ledermann, "Ovarian cancer", Lancet., vol. 384, pp. 1376-1388, 2014.

[20] Y. Lee, A. Dutta, "MicroRNAs in Cancer", Annu. Rev. Pathol., vol. 4, pp. 199-227, 2009. https://doi.org/0.1146/annurev.pathol.4.110807.092222

[21] J. Akers, V. Ramakrishnan, R. Kim, J. Skog, I. Nakano, S. Pingle, J. Kalinina, W. Hua, S. Kesari, Y. Mao, X. Breakefield, F. Hochberg, E. Van Meir, B. Carter and C. Chen, "MiR-21 in the extracellular vesicles (EVs) of cerebrospinal fluid (CSF): A platform for glioblastoma biomarker development", PLoS One, vol. 8, no.10, 2013. https://doi.org/10.1371/journal.pone.0078115.

[22] E. H. Mahmoud, A. Fawzy, R. A. A. Elshimy, "Serum MicroRNA-21 Negatively Relates to Expression of Programmed Cell Death-4 in Patients with Epithelial Ovarian Cancer", Asian Pac J Cancer Prev., vol. 19, pp. 33-38, 2018. https://doi.org/10.22034/APJCP.2018.19.1.33.

[23] D. A. Forero, Y. González-Giraldo, L. J. Castro-Vega, G. E. Barreto, "qPCR-based methods for expression

analysis of miRNAs", BioTechniques, vol. 67, pp. 192-199, 2019. https://www.doi.org/10.2144/btn-2019-0065.

[24] C. M. Hindson, J. R. Chevillet, H. A. Briggs, E. N. Gallichotte, I. K. Ruf, B. J. Hindson, R. L. Vessella, M. Tewari, "Absolute quantification by droplet digital PCR versus analog real-time PCR", Nat. Methods, vol. 10, pp. 1003-1005, 2013.

[25] Y. D. Ma, W. H. Chang, K. Luo, C. H. Wang, S. Y. Liu, W. H. Yen, G. B. Lee, "Digital quantification of DNA via isothermal amplification on a self-driven microfluidic chip featuring hydrophilic film-coated polydimethylsiloxane", Biosens. Bioelectron, vol. 99, pp. 547-554, 2018. https://doi.org/10.1016/j.bios.2017.08.026.

[26] K. E. Thane, A. M. Davis, A. M. Hoffman, "Improved methods for fluorescent labeling and detection of single extracellular vesicles using nanoparticle tracking analysis", Sci. Rep., vol. 8, 2019.

[27] Q. Zhu, Y. Gao, B. Yu, H. Ren, L. Qiu, S. Han, W. Jin, Q. Jin, Y. Ma, "Self-priming. compartmentalization digital LAMP for point-of-care", Lab Chip., vol. 12, pp. 4755-4763, 2012.

.